Chapter 5

Collimation system

S. Redaelli[1*], *R. Bruce*[1], *A. Lechner*[1] *and A. Mereghetti*[1]

[1]CERN, Accelerator & Technology Sector, Switzerland
[*]Corresponding author

5 Collimation system

5.1 The LHC multi-stage collimation system

5.1.1 Introduction

A variety of processes can cause unavoidable beam losses during normal and abnormal beam operation. Because of the high stored energy of about 700 MJ and the small transverse beam sizes, the HL-LHC beams are highly destructive. Even a local beam loss of a tiny fraction of the full beam in a superconducting magnet could cause a quench, and larger beam losses could cause damage to accelerator components. Therefore, all beam losses must be tightly controlled. For this purpose, a multistage collimation system has been installed [1][2][3][4][5][6][7][8], to safely dispose of beam losses. Unlike other high-energy colliders, where the main purpose of collimation is typically to reduce experimental backgrounds, the LHC and the HL-LHC require efficient beam collimation during all stages of operation from injection to top energy. The requirement to operate efficiently and safely with high-intensity hadron beams at small colliding beam sizes provides significant challenges, which drive the key design aspects of the collimation system at the HL-LHC.

The HL-LHC poses increased challenges to the collimation system. The LHC collimation system was designed to safely withstand beam lifetime drops down to 0.2 h during 10 s at 7 TeV, corresponding to peak losses of up to 500 kW, which increase to 945 kW for the HL-LHC. The ion beam upgrade, with the target of storing more than 20 MJ at 7 Z TeV and producing luminosities above 7×10^{27} cm^{-2} s^{-1} [9], is also very demanding for beam collimation. The collimation system must be upgraded on various fronts to cope with more demanding operation challenges. It is clear that the lifetime control and optimization of beam halo losses will also be crucial for the LHC upgrade (see also Section 5.4). Three main pillars of the collimation system upgrade for the HL-LHC can be identified:

- Re-design of the collimation system of incoming and outgoing beams in the upgraded insertion regions IR1 and IR5.
- Improved protection of the Dispersion Suppressor (DS) regions around IR7 and IR2 to mitigate increased local beam losses.
- Reduction of the collimator-induced impedance to allow the operation with higher brightness beams in the HL-LHC.

Note that the HL-LHC also relies significantly on operational efficiency as it is based on operation with levelled luminosity, so that it becomes even more important to minimize time spent outside physics operation. Improvements of the collimator setup time and minimization of downtimes from collimator faults also call for a consolidation of the present system. This can be seen as an essential “fourth pillar” of the system in light of

the HL-LHC operation. Indeed, to meet the new challenges, the HL-LHC collimation system builds on the existing LHC collimation system, with the addition of several upgrades.

It is also noted that, as a part of the upgrade of the collimation betatron cleaning, two new items were integrated in the baseline upgrade of WP5: hollow electron lenses and crystal collimation. In the previous HL-LHC baseline upgrade [10], WP5 budgets covered the R&D phase for these items, but not their implementation that was subject to the assessment of needs for these technologies and of the demonstration of their feasibility. After several years of studies, these items were incorporated in the WP5 upgrade baseline in Dec. 2019 by the CERN management following the 4th Cost & Schedule review [11]. The incorporation into the baseline was possible thanks to the in-kind contribution by Russia to the HL-LHC project. These new advanced collimation concepts are described in Section 5.6.

5.1.2 The LHC collimation system

The backbone of the HL-LHC collimation system will remain, as for the current LHC, the betatron (IR7) and momentum (IR3) cleaning systems installed in two separated warm insertions [1]. A very efficient halo cleaning is achieved by very precisely placing blocks of materials close to the circulating beams, while respecting a pre-defined collimator hierarchy that ensures optimum cleaning in a multi-stage collimation process. This is illustrated schematically in Figure 5-1 and the list of the LHC collimation system devices is given in Table 5-1.

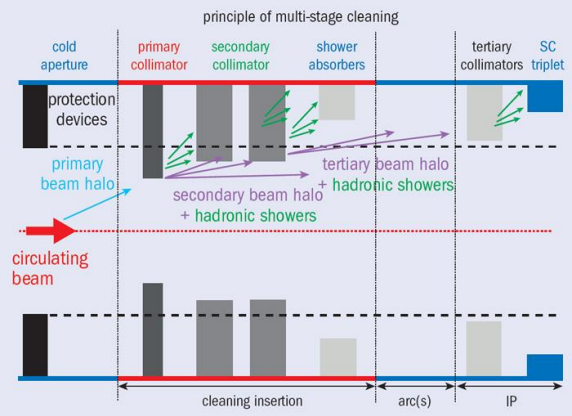

Figure 5-1: Schematic illustration of multi-stage collimation cleaning at the LHC.

Most collimators consist of two movable blocks referred to as ‘jaws’, typically placed symmetrically around the circulating beams. The present IR7 system, used in the LHC proton operation in Run 1 (2010–2013) [12] and Run 2 (2015–2018) [13], provided a cleaning efficiency above 99.99% [2], i.e. it ensures that less than 10^{-4} of primary beam losses reach the superconducting magnets. Highest losses occur in the DSs around IR7, while the rest of the cold elements around the ring are typically a factor 10 lower. The system was significantly upgraded already in the first LHC long shutdown (LS1, between 2013 and 2015), by replacing 18 collimators with new ones based on the new integrated-BPM design (see below), by improving the passive protection of warm magnets in IR3, and by adding 8 new physics debris collimators in IR1/5 [14]. About 30-40% of the present system will have to remain operational throughout the HL-LHC era as part of the collimation system. These collimators will need to be kept fully operational to ensure an efficient operation of the HL-LHC.

The initial LHC collimator design has been improved by adding two beam position monitors (BPM pickups) on both extremities of each jaw [21][22][23][24]. Eighteen operational collimators (16 TCTP and 2 TCSP) were already upgraded with this new design during LS1 [14]. Four additional prototypes with BPMs were included in the system in various yearly stops of the LHC [25][26][27][28]. This concept allows for fast collimator alignment as well as a continuous monitoring of the beam orbit at the collimator with the possibility to interlock the readout of the beam position. The BPM pickups have improved significantly the collimation

performance in terms of operational flexibility and β^* reach [13][29]. In particular, this was one of the key ingredients that allowed β^* values down to 25 cm in 2018 [19][20][29]. The BPM design is now applied to all new collimators regardless of the jaw material.

Table 5-1: Collimators for the LHC Run 2, starting in 2015. For completeness, injection and dump devices are also listed.

Functional type	Name	Plane	Number	Material
Primary IR3	TCP	H	2	CFC
Secondary IR3	TCSG	H	8	CFC
Absorber IR3	TCLA	H, V	8	Inermet 180
Primary IR7	TCP	H, V, S	6	CFC
Secondary IR7	TCSG	H, V, S	22	CFC
Absorber IR7	TCLA	H, V, S	10	Inermet 180
Tertiary IR1/IR2/IR5/IR8	TCTP	H, V	16	Inermet 180
Physics debris absorbers IR1/IR5	TCL	H	12	Cu, Inermet180
Dump protection IR6	TCDQ	H	2	CFC
	TCSP	H	2	CFC
Injection protection (transfer lines)	TCDI	H, V	13	Graphite
Injection protection IR2/IR8	TDI	V	2	hBN, Al, Cu/Be*
	TCLI	V	4	Graphite, CFC
	TCDD	V	1	Copper

*In 2016, the TDI collimator absorbing materials were changed to Gr, Al, CuCrZr

5.2 Baseline upgrades to the LHC collimation system

In this Section, for each upgrade pillar, we present the WP5 upgrade baseline. The two new upgrade items that were added to the WP5 baseline in Dec. 2019 – hollow electron lenses and crystal collimation – are discussed in Section 5.6.

The detailed scope of the collimation baseline upgrade can be summarized as follows (details of all items are discussed in the subsequent Sections):

- IR collimation upgrade:
  - 4 tertiary collimators per beam and per high-luminosity IR are needed to protect the inner triplet and the matching section from losses on the incoming beam, amounting to a total of 16 tertiary collimators.
  - 3 physics debris collimators and 3 fixed masks per beam and per high luminosity IR are needed to protect matching section and DS from collision debris in IR1/5, amounting to a total of 12 collimators and 12 masks.

Note that 8 collimators can be recuperated from the existing pool of operational collimators (i.e., the 8 tertiary collimators presently used in IR1 and IR5, built in LS1) or spare collimators of type "TCTP" (Inermet 180 jaws with pick-ups). Thus, 20 rather than 28 new collimators are needed to be designed and built.

The IR collimation upgrade is deployed during LS3 when IR1/5 will be upgraded for the HL-LHC.

- Dispersion suppressor upgrade:

- Addition of DS collimators TCLD in the DSs around IR7 for proton and ion operation, with the addition of 11 T dipoles: 1 collimator per beam in cell 9 per side of P7;
- Addition of DS collimators TCLD in the DSs around IR2 for ion operation, without 11 T dipoles: 1 collimator per beam in cell 11 at each side of P2 at the location of the connection cryostat.

Note that the losses in the DSs of IR1/5 during ion operation are mitigated by local bumps in the DS that move losses to the location of the connection cryostat, without need for dedicated collimators. The complete DS collimation upgrade takes place in LS2.

- Low-impedance upgrade:
  - Replacement of 9 secondary collimators per beam, out of the present 11 per beam, with a new low-impedance design; in total 18 new low impedance collimators.
  - Contribution to the construction on new primary collimators (renewed under the Consolidation project) by providing the low-impedance material for the jaws.

  The low-impedance upgrade of the system takes place in two phases:
  - Four new secondary collimators and two primary collimators per beam are installed in LS2.
  - The rest of the five secondary collimators per beam are installed in LS3.

The detailed list of collimators to be produced for the WP5 upgrade of the collimation system is given in Table 5-2.

Two baseline changes have taken place with respect to the previous TDR:

- The change of location for the TCLD collimators around IR7, from cell 8 to cell 9.
- The scope reduction by 4 units of the low-impedance collimators to be installed in LS3. In addition, a further change of scope – the WP5 contribution to the procurement of low-impedance material for the consolidated primary collimators – was also approved [18].

Table 5-2: List of the new HL-LHC collimators. The IR upgrade will require 28 operational collimators in IR1/5, 8 of which are planned to be recuperated from the existing TCTP collimators.

Collimator description	**Names**	**LS2 installation**			**LS3 installation**		
		Operational	**Production**	**Spares**	**Operational**	**Production**	**Spares**
Tertiary collimators	TCTPXH, TCTPXV, TCTPM, (TCTP)	--	--	--	16	12	2
Physics debris collimators	TCLP, TCLPX, (TCTP)	--	--	--	12	8	2
Physics debris collimator masks	TCLM	--	--	--	12	12	3
DS collimators	TCLD	4	4	1	--	--	--
Low-Impedance secondary collimators	TCSPM	8	8	2	10	10	2

5.3 Collimation upgrade in the high-luminosity interaction regions: IR Collimation

With the increased beam intensity and luminosity of the HL-LHC, the protection of the IR superconducting magnets and experiments becomes even more challenging. In order to provide adequate protection, the HL-LHC collimation layout in IR1 and IR5 includes two pairs of TCTs (horizontal and vertical) on each incoming

beam, as well as three physics debris absorbers (TCLs) and three fixed masks on each outgoing beam. This is illustrated in Figure 5-2, showing the HL-LHC layout in IR1 together with the nominal LHC layout. The layout in IR5 is similar and contains the same upgrades. The upgrades for the incoming and outgoing beams, as well as the newly developed collimator designs, will be discussed in more detail in the following Sections.

5.3.1 Upgrades to the collimation of the incoming beam in the experimental IRs

The present tertiary collimators (target collimator tertiary with pick-up, TCTP) are located at positions that protect the triplet; in order to provide the necessary absorbance, they are made of a heavy tungsten alloy (Inermet 180). They effectively protect the elements downstream, but are not robust against high beam losses, in particular during very fast beam failures that might occur if the beam dumping system does not trigger synchronously with the abort gap (an asynchronous beam dump). With the increase in bunch intensity of the HL-LHC, this accident scenario becomes even more critical. Settings margins are added to the collimator hierarchy to minimize the risk of exposure of these collimators to beam losses in case of such failures [3][19]. These margins have been reduced in Run 2 using a new optics with a specially matched phase advance between the extraction kickers and the TCTs [20], which was used to push further the β^* performance of the LHC. A TCT design with improved robustness would allow an alternative way to reduce the hierarchy margins without introducing constraints on the optics. This gives more flexibility in the optics design, which is useful in particular for the HL optics baseline that features many other constraints.

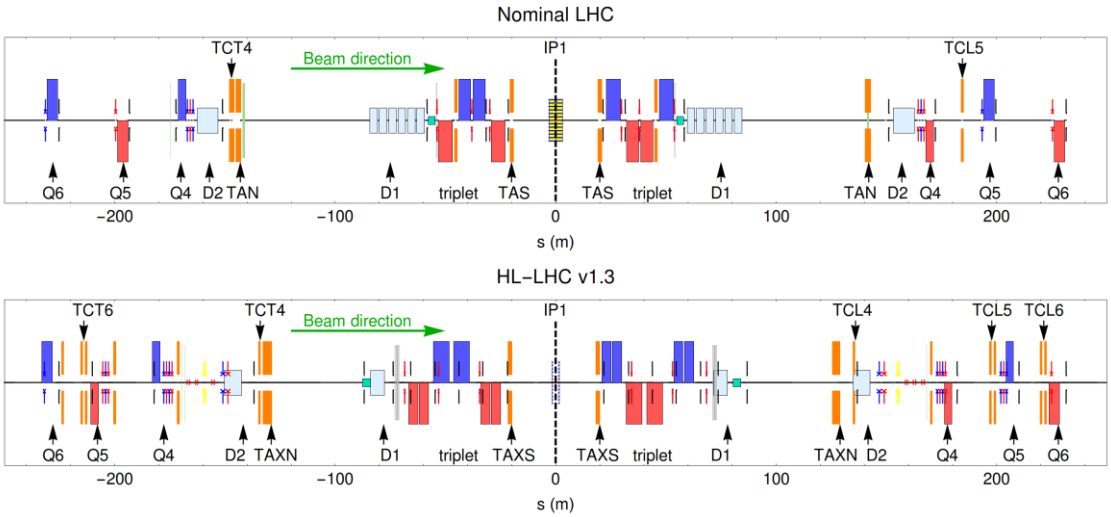

Figure 5-2: Schematic layout in experimental insertion IR1 for LHC (top) and the HL-LHC v1.3 (bottom). Collimators are indicated in orange, quadrupoles in blue and red for the two polarities, and dipoles in cyan.

The experimental experience of beam impacts on collimator material samples at HiRadMat [36], where several new materials were studied, indicates that molybdenum graphite (MoGr) can improve the TCTP robustness by a factor of several hundreds, while copper-diamond (CuCD) features higher density (and hence better cleaning efficiency) and larger electrical conductivity and still gives about a factor 15 improvement in robustness [37]. In order to keep a good absorption, the baseline is therefore to use CuCD in the horizontal TCTs, while the vertical ones are still made of Inermet 180, since the critical losses from an asynchronous beam dump occur only in the horizontal plane.

In addition to improvements from increased robustness, the HL-LHC layout has additional aperture constraints [2][3] because the optics functions at the magnets up to Q5 planned at the HL-LHC reduce the normalized aperture. Thus, additional tertiary collimators are required in IR1/IR5 to protect the Q4 and Q5 quadrupole magnets. The present baseline includes a pair of new TCTP collimators in front of Q5, including one horizontal and one vertical, and another pair of TCTPs just upstream of the TAXN to protect the triplet, as for the nominal LHC.

The expected beam losses in the experimental insertions have been verified in simulations. Tracking simulations using SixTrack [38][39] show that the proposed layout provides adequate protection of all magnets against cleaning losses [40][41]. Simulations of asynchronous beam dumps show that no direct losses are to be expected on the magnets, and losses of up to about 2×10^{10} protons [42] could occur on the TCTs [43]. Those losses are spread-out secondary protons, scattered out of upstream collimators, about a factor 5 below the onset of plastic deformation even for Inermet 180. This result relies on a matched fractional phase advance below 30° between the extraction kickers and the TCTs, as implemented in the HL-LHC v1.3. Under these conditions the heat deposition in SC magnets and in experimental detector is quite safe with respect to damage.

5.3.2 Outgoing beam cleaning: physics debris in the matching section

The collimators on the outgoing beams, downstream of the high-luminosity experiments, must intercept both scattered primary beam particles and secondary particles generated by the collisions, in order to protect the magnets downstream. The protection of the triplet from luminosity debris is discussed in Chapter 10, and here the focus is instead on the protection of the matching section. In Run 1, protection of the matching section was done by a single horizontal collimator in Cell 5, called TCL5. For Run 2, the system was upgraded with additional TCLs in cells 4 and 6 (8 new collimators), to cope with the higher luminosities and requirements from forward-physics experiments.

In the HL-LHC, the levelled luminosity of 5 to 7.5 $\times 10^{34}$ cm^{-2} s^{-1} will be about a factor four higher than the peak achieved during Run 2 in the LHC, which is a significant challenge for the collimation of physics debris. In addition, the absorber TAXN (the upgrade of the TAN, see Chapter 8) is less effective, in fact, because of the geometry of the reference trajectory and crossing angle, a significantly larger fraction of the scattered particles can pass through its opening than in the LHC [47].

In order to cope with these challenging conditions, several improvements are foreseen for the HL-LHC. The TCL4 needs to be upgraded to have thicker jaws [47] in order to intercept a larger fraction of the particles that have passed through the TAXN opening. This new collimator is called TCLX, and a sketch of the increased coverage in the transverse plane, compared with the present, thinner TCL, is shown in Figure 5-3. It should be noted that the jaw material is changed from copper to tungsten heavy alloy for better protection. In addition, fixed masks have to be installed on the IP side of Q4, Q5, and Q6, with the aperture well aligned and matching the beam screen of each magnet. Furthermore, the TCL5 and TCL6 are still needed. Using this new layout, the highest power loads in any magnet coil in the matching section stays below 1 mW/cm^3 [46], which is far below the estimated quench limits. It should be noted also that the TCTs play a role in protecting the incoming beam bore from the collision debris.

5.3.3 Collimator designs for IR collimation

The design of the new IR collimators is challenging. Due to the larger β-functions in the HL-LHC high-luminosity insertions, the TCTs and TCLs in cell 4 have to be opened to rather large gaps in mm to achieve the smaller normalized design openings in σ. To keep a maximum operational flexibility, it is thus demanded that the stroke should be as large as 15 σ for the baseline optics with β^*=15 cm. In this case, a half gap of 34 mm is needed for the most critical, vertical, collimator, which goes up to 40 mm for flat optics [49][50]. The half gap is limited to 30 mm in the present collimator design, so modifications are necessary. Similar considerations apply also to the TCLs. This calculation includes imperfections from orbit, optics, and ground motion, but also a gain of several mm thanks to remote alignment capabilities, described in Chapter 15. Without the gain from the new remote alignment system, the present design would have to be changed to meet the design specifications in terms of jaw strokes.

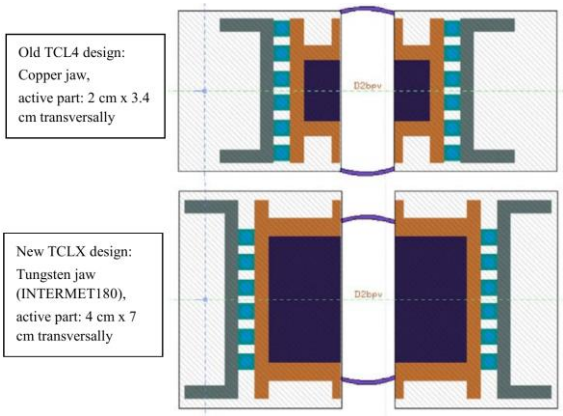

Figure 5-3: A schematic of the transverse cross-section of the present TCL design, as implemented in FLUKA (top), together with a first guess on the TCLX design (bottom), including thicker jaws, where the jaw material should be changed from copper to tungsten heavy alloy. Figure from Ref. [48].

In addition, the region in cell 4 between the D2 separation dipole and the TAXN, where the beams are recombined in a common vacuum chamber, is particularly critical from the integration point of view. In order to provide the needed stroke and still fit in the horizontal space, a new two-in-one collimator design for the horizontal TCT and the TCL4 has been developed. In this design, a single vacuum tank houses at the same location the movable jaws acting on one beam and the vacuum chamber of the opposing, non-collimated, beam. Details like the vacuum coupling of the two beams as well as the impedance budget of this design need to be studied in detail, but this proposed solution seems suitable for the HL-LHC. A 3D model of this design is shown in Figure 5-4. For the vertical TCT in Cell 4, a two-in-one design is not needed, however, a special design still has to be developed to implement the larger stroke up to 40 mm. These collimators with special designs will all have a letter "X" in the name. A summary of the technical key parameters is given in Table 5-3 for the different collimator types, and Figure 5-5 shows a 3D model of the proposed layout in the region between the TAXN and the D2.

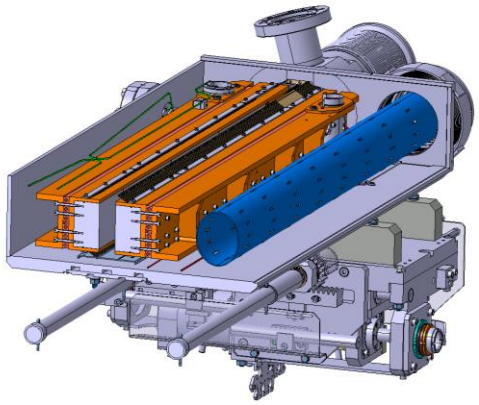

Figure 5-4: Design of new two-in-one collimator with a common vacuum tank housing both the movable jaws (left part) and the vacuum chamber of the opposing beam.

For the TCLs in cell 5 and 6, and the TCT in Cell 6, the standard 30 mm stroke of the present collimator design is sufficient. It is important to note that some of these collimators should re-use the present TCTP collimators with BPM that are essentially of the same design and using Inermet 180 as active material. It is believed that up to 8 collimators can be recuperated from those built for the present LHC (units installed in the machine or operational spares). It is planned to use these collimators in the vertical TCT slot in Cell 6 (not exposed to beam dump failures at top energy) and as single-beam horizontal TCLs in cells 5 or 6 that are at settings above 10 σ. For the horizontal TCTs in Cell 6, new collimators using CuCD as active material will be

built, as well as the remaining TCLs. A total of 20 movable collimators and 12 fixed masks have to be built for the IR1 and IR5 installations in the HL-LHC.

Table 5-3: Equipment parameters of the new TCTs and TCLs to be installed in cell 4.

Characteristics	Units	TCLX	TCTPXH	TCTPXV
Jaw active length	mm	1000	1000	1000
Jaw material	-	Inermet 180	Copper-diamond	Inermet 180
Flange-to-flange distance	mm	1556	1556	1480
Number of jaws	-	Two	Two	Two
Orientation	-	Horizontal	Horizontal	Vertical
Number of motors per jaw	-	Two	Two	Two
Number of BPM buttons per jaw	-	Two	Two	Two
RF damping	-	Fingers	Fingers	Fingers
Cooling of the jaw	-	Yes	Yes	Yes
Cooling of the vacuum tank	-	Yes	Yes	Yes
Maximum half gap	mm	> 39	> 33	> 40
Stroke across zero	mm	>5	>5	>5
Angular adjustment	-	Yes	Yes	Yes
Jaw coating	-	No	No	No
Transverse jaw movement (fifth axis)	-	No	No	No

Despite being less critical because of the larger β^* values, upgraded TCTPs are under consideration also for IR2/8 because various luminosity scenarios in these IRs require the usage of tertiary collimators, although at relaxed settings compared to IR1 and IR5. For the time being, new collimators in IR2/8 are not considered part of the baseline.

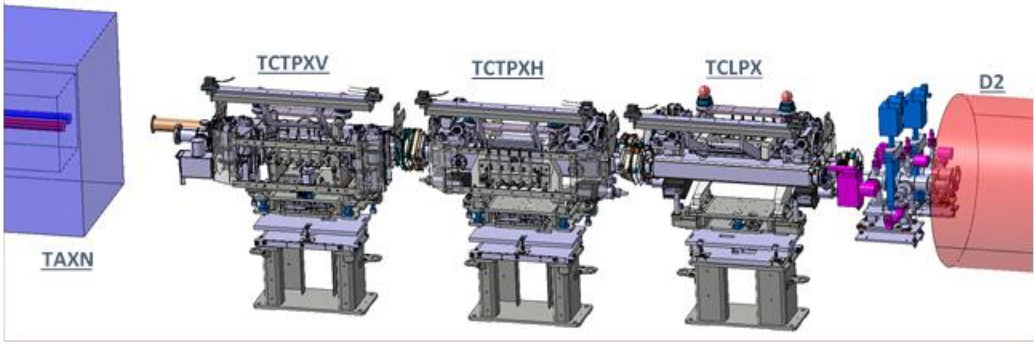

Figure 5-5: Layout in the region in Cell 4 between the TAXN and the D2.

5.4 Dispersion suppressor collimation upgrades

5.4.1 Introduction

The necessity of cleaning upgrades in the DSs for the HL-LHC is primarily driven by the increased risk of quenches arising from off-momentum losses. The source of dispersive losses can be halo particles intercepted in the collimation system or collision products from the interaction points. Extensive tracking and shower simulations, as well as experimental quench tests were carried out in Run 1 and Run 2 in order to determine the expected power loads and quench margins both for proton and heavy ion operation. The results, summarized in the following Sections, indicate that upgrades of the collimation cleaning hardware are needed in the DSs next to IR7 (for Pb operation and probably also for proton operation), and in the DSs around IR2 (for Pb operation). Note that steering of loss peaks into the connection cryostats of IR1 and IR5 successfully mitigates losses in these IR's without the need for hardware upgrades.

The DSs around IR7 are the main bottleneck in the LHC in terms of collimation leakage both for protons and heavy ions. The design goal for the present LHC collimation system was to avoid quenches and beam dumps for a beam lifetime of 0.2 h for up to 10 s, or 1 h for extended time periods [1]. The same specification is maintained for the HL-LHC, which implies that the cleaning system must sustain a higher power loss due to the higher beam intensity. The need for upgrades depends on the level of losses eventually encountered in the HL-LHC operation and the quench limit of superconducting magnets. In this design phase, where there are significant uncertainties for the scaling to higher energy, it is important to take appropriate margins. To mitigate the risk of quenches due to IR7 leakage, it is foreseen to add local collimators, referred to as TCLDs, in the DSs, where the dispersion has already started rising. In order to make space for the new collimators, it is envisaged to replace, for each TCLD, an existing main dipole with two shorter 11 T dipoles [53].

The need for a cleaning upgrade in the DS also arises for heavy ion collisions in IP2. Secondary ion beams with different magnetic rigidity are created, which are lost in the adjacent DS and would induce a quench of magnets at the HL-LHC Pb-Pb target luminosity of $7 \times 10^{27} \mathrm{cm}^{-2}\,\mathrm{s}^{-1}$ [9]. A similar solution, based on TCLDs, will therefore be adopted in IR2, with the difference that the collimator will be installed at the location of the connection cryostat in Cell 11, thanks to a dedicated cryogenics bypass.

5.4.2 Dispersion suppressors around IR7

A small fraction of protons interacting with the collimators in IR7 escapes from the IR with a modified magnetic rigidity. These protons, which are mainly single diffractive protons emerging from the TCPs, represent a source of local heat deposition in the cold DS magnets downstream of IR7, where the dispersion starts to increase (see [52] and references therein). These losses are among the highest losses in cold magnets around the ring. In case of large drops in the beam lifetime, in particular for the case of the HL-LHC where the stored energy is almost doubled compared to the nominal LHC, the impacted magnets risk quenching and the beams should be dumped before based on the BLM readings. This would result in costly downtime and reduced the HL-LHC availability and have a negative impact on physics production. The same applies to secondary ion fragments produced in IR7 collimators during heavy ion operation. Although the intensities of heavy-ion beams are lower, they undergo numerous nuclear and electromagnetic interactions with the material of the primary collimators, creating an abundance of secondary ions with different mass and charge. Collimation of heavy-ion beams is therefore much less efficient than that of proton beams.

In order to probe the acceptable losses in the DSs around IR7, experimental quench tests have been performed with protons and Pb ions at different beam energies between 3.5 TeV and 6.5 TeV [54][55][56][57][58][59]. The proton quench tests, in particular the latest one at 6.5 TeV, did not result in a quench [58], however, the heavy-ion test with a 6.37 Z TeV Pb beam resulted in a quench of the dipole MB.B9L7 [59][60]. Table 5-4 summarizes the corresponding peak power densities in the MB coils, obtained with FLUKA [61][62] shower simulations. The FLUKA simulations were based on multi-turn tracking simulations [63][64] performed with the FLUKA-SixTrack coupling [60][65][66], for the configuration deployed in the quench tests [67]. The table also includes results of another quench test performed in IR5, based on Bound-Free Pair Production (BFPP) ions produced by the collision of Pb beams at 6.37 Z TeV [57]. This test also achieved a dipole quench. The losses exhibited different time profiles in the different tests, which affected the minimum power density needed to induce a quench. According to electro-thermal simulations, the minimum quench power density in $\mathrm{mW/cm^3}$ can be a factor of two, or more, higher if the losses are rising than if the losses are constant in time. This can possibly explain why the maximum power density was found to be somewhat higher for the Pb collimation quench test than for the BFPP test. It should nevertheless be stressed that these numbers are computed in complex simulations that have a non-negligible range of uncertainty and therefore a certain margin needs to be considered for the power density estimates reconstructed by the simulations.

Table 5-4: Simulated peak power densities in MB dipole coils for different quench tests. The values are radially averaged over the coil radius. The results for the collimation quench tests include an empirical correction based on BLM signals, which accounts for the underestimation of particles leaking to the DS.

Loss term	**Beam particles**	**Energy**	**Time profile of losses**	**Quench**	**Reconstructed maximum power density MB coils**	**Complexity of simulations**
Betatron collimation leakage (DS next to IR7)	Protons	6.5 TeV	Losses rising for 5 sec	No	23 mW/cm3	High
Betatron collimation leakage (DS next to IR7)	Pb ions	6.37 ZTeV	Losses rising for 12 sec	Yes	25-30 mW/cm3	High
Secondary ions from IP (DS next to IR5)	Pb ions	6.37 ZTeV	Losses rising for 20 sec	Yes	20 mW/cm3	Low-medium

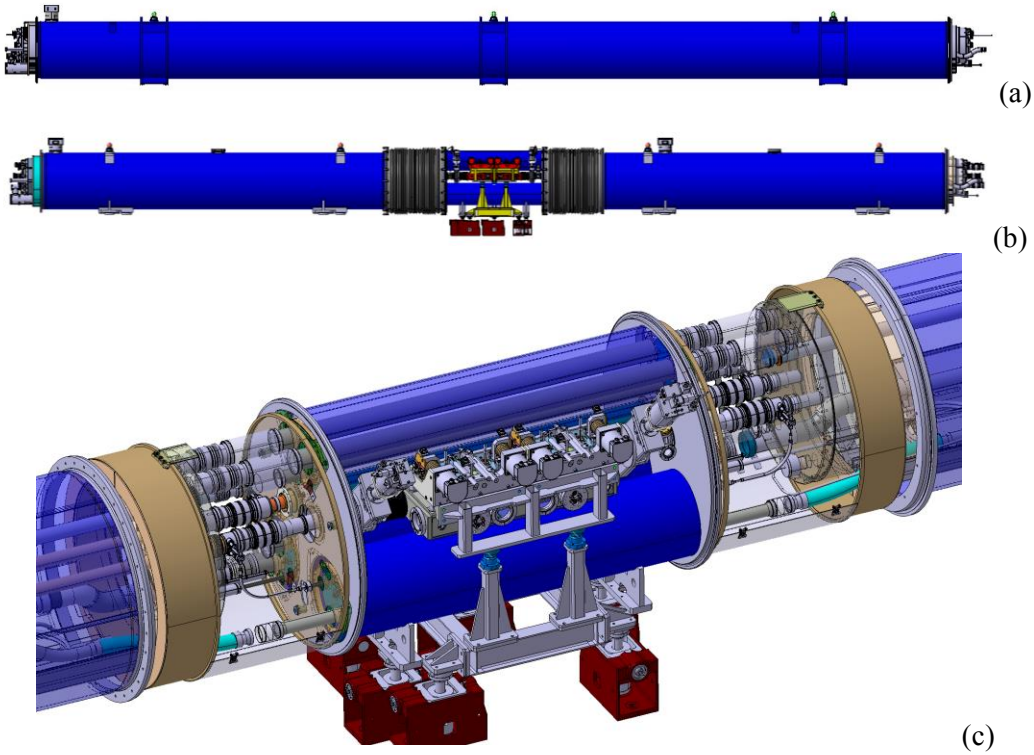

Figure 5-6: (a–b) Schematic view of the assembly of two shorter 11 T dipoles with a collimator in between, which can replace one standard main dipole. (c) 3D model showing the collimator (in grey, at the centre), the two dipole cryostats and the connection cryostat (courtesy of L. Gentini).

For comparison, Table 5-5 summarizes FLUKA results of the peak power density in DS magnets for the HL-LHC beam parameters at 7 Z TeV, i.e. 2760 proton bunches with a bunch intensity of 2.3×10^{11} and 1248 Pb bunches with a bunch intensity of 2.1×10^{8} ions [68] (previous results can be found in Refs. [69] [70] [71] [72]). These proton beam parameters are only expected in Run 4 whereas the upgraded ion beams are already expected in Run 3. The table shows results [69] for different layouts, including the case without TCLD and with TCLD at the MB.B8 in Cell 8 or at the MB.A9 in Cell 9. Inputs are from Refs. [73] [74]. The collimator settings for protons (ions), specified for a normalized emittance of 3.5×10^{-6} m rad, are: TCP at 5.7σ (6.0σ), TCSGs at 7.7σ (7.0σ), TCLAs at 10σ (10σ) and TCLD at 14σ (14σ) [63][64].

Table 5-5: Simulated peak power densities in superconducting coils of DS magnets in cells 8/9 and 11, expressed in mW/cm^3, respectively for a beam energy of 7 Z TeV. The values are radially averaged over the coil radius. Results for different layouts are shown (no TCLD, TCLD at the location of the present MB.B8 and the MB.A9). The nominal HL-LHC beam parameters are used and an empirical correction factor of 3 accounting for the underestimation of particles leaking to the DS in the simulation is applied.

		PROTONS (mW/cm^3)					**IONS (mW/cm^3)**				
		Cell 8/9			**Cell 11**		**Cell 8/9**			**Cell 11**	
		MB	**MQ**	**11T**	**MB**	**MQ**	**MB**	**MQ**	**11T**	**MB**	**MQ**
No TCLD	0.2 h	21	9.9	-	12	13	57	27	-	57	36
	1 h	4.2	2.0		2.4	2.6	11	5.4	-	11	7.2
MB.B8	0.2 h	6.6	8.1	11	8.7	13	5.4	15	21	36	33
	1 h	1.3	1.6	2.2	1.7	2.6	1,1	3	4.2	7.2	6.6
MB.A9	0.2 h	6.0	8.1	48	< 0.3	< 0.3	6.0	3.6	33	< 0.003	< 0.003
	1 h	1.2	1.6	9.6	< 0.06	< 0.06	1.2	0.7	6.6	< 0.0006	< 0.0006

For Pb ions, the simulations indicate that, with the present DS layout without TCLD, the peak power density in the most loaded IR7 DS magnet reaches almost 60 mW/cm^3 during a 0.2 h lifetime drop. This is higher than the peak power density reached in both the BFPP and the Pb collimation quench tests at 6.37 Z TeV, indicating that a cleaning upgrade is needed at 7 Z TeV, with magnets with even lower quench limits that at 6.5 ZTeV. A similar conclusion can be reached by simply scaling the acceptable power load determined in the Pb collimation quench test.

It should be recalled that full mitigation of the losses from heavy-ion collimation would ideally require two collimators on each side of IR7. This solution would consistently cure the two main loss clusters in cell 8/9 and cell 11, and in addition would suppress efficiently the off-momentum halo that leaves IR7 after interactions with the collimators, causing losses in other locations around the ring. As a result of the re-baselining in 2016, it was decided to have only 1 TCLD collimator per beam. This decision was to a large extend determined by cost constraints, but also by the clear understanding that the need for the additional TCLD collimators per DS side was not 100% certain and that it would not have been possible to produce more than 4 new dipoles in time for installation in LS2. Possible further installations might be considered later on. The results in

indicate that, if the TCLD is located in Cell 8, a risk remains that a quench occurs in Cell 11, where the collimator is less effective. A much better cleaning in Cell 11 can be achieved by placing the TCLD in Cell 9, but with the disadvantage that the heat load in the 11 T magnet upstream of the collimator increases by about a factor 2 [48 mW/cm^3 during proton operation instead of 21mW/cm^3 during ion operation]. Recently updated studies [77] suggest that the quench level of the 11 T magnets is significantly higher than that of the MB, reaching about 70 mW/cm^3 [78]. The higher heat load in the 11 T magnets seems therefore acceptable, although the remaining margin is moderate.

For protons, the predicted peak power density for the HL-LHC beams with a 0.2 h lifetime and without TCLD is about a factor of three lower than that for ions, reaching about 20 mW/cm^3 at 7 TeV. Nevertheless, this value is comparable to the power density reached in the steady-state BFPP quench test at 6.37 *Z* TeV. Based on these results and considering the simulation uncertainty, it is estimated that the TCLDs might be needed in Run 4 even for safe proton operation. Like for ions, one can achieve a better cleaning if the collimator is located in Cell 9. The addition of a TCLD in Cell 9 improves the loads on standard dipoles by more than a factor 3, bringing losses to the level of 6 mW/cm^3, but again with the disadvantage of a locally higher heat load in the 11 T. For a 12 minutes lifetime, the power density in the 11 T coils is predicted to reach almost 50 mW/cm^3. It is to be noted that this power density is reached in the 11 T magnet upstream of the TCLD and hence the TCLD settings have no influence on this value. It is also worth noting that the 50 mW/cm^3 in the 11 T coils is about a factor of two higher than that in the MB.A9 replaced by the 11 T magnets. This can mainly be attributed to the higher dipole field, which leads to an enhancement of off-momentum proton impacts on the 11 T beam screen as compared to the MB. The predicted power density in the 11 T is still lower than the

above quoted 11 T quench level, although a smaller safety margin remains. Losses are localized towards the end of the 11 T dipole upstream of the TCLD and various mitigation measures are under study to reduce further the load (optimized alignment of the 11 T dipole, effect of local bumps).

In conclusion, it seems at this stage that one TCLD per beam is acceptable for the performance. On the other hand, this should be reviewed later in light of the Run 3 performance.

5.4.3 Dispersion suppressors around IR2

Secondary ion beams produced with a modified magnetic rigidity are generated in ion collisions and represent a source of local heat deposition in the adjacent DS regions where the dispersion function starts rising. The dominating processes are bound-free pair production (BFPP), where electron–positron pairs are created and one (BFPP1) or two (BFPP2) electrons are caught in a bound state of one of the colliding nuclei, thus changing its charge, and 1- or 2-neutron electromagnetic dissociation (EMD1 and EMD2) where one nucleus emits one or two neutrons, thus changing mass. An example of ion beams produced in collisions of $^{208}Pb^{82+}$ nuclei in IR2 is given in Figure 5-7.

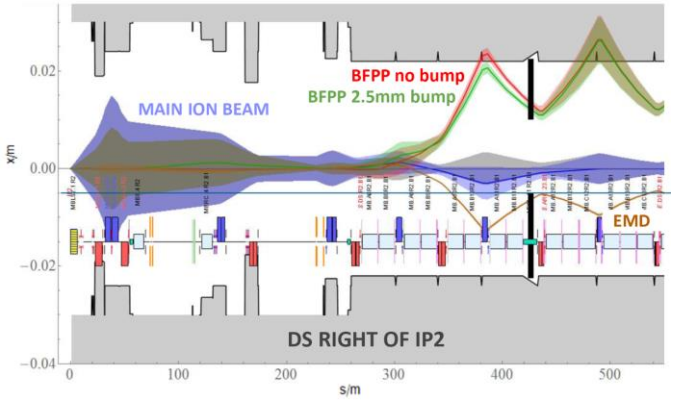

Figure 5-7**:** 1 σ envelope of the main Pb^{82+} beam (violet) together with the dispersive trajectories of ions undergoing BFPP1 (red) and EMD1 (brown), coming out of IP2. Black lines indicate the TCLD jaws. The green line indicates the shifted BFPP1 orbit using a closed orbit bump, which is necessary to intercept the beam with the collimator. The EMD1 beam can be intercepted with the other jaw.

After the LS2 ALICE upgrade, aiming at a peak luminosity of 7×10^{27} cm^{-2} s^{-1} (about seven times higher than the nominal one), the dominant BFPP1 beam can carry about 180 W, resulting in a power load in the coils of the MB.B10 dipole of about 50 mW/cm^3 [71][81][82] on both sides of ALICE. Similar ion losses also occur in the DS regions around ATLAS and CMS (see next Section).

A beam loss experiment carried out during the 2015 Pb-Pb run at 6.37 Z TeV [57] confirmed the long-standing presumption that BFPP1 ions risk to quench magnets [79][80]. The experiment was carried out around CMS because of the higher peak luminosity than in ALICE. During standard operation, special bumps were deployed around ATLAS and CMS to steer the BFPP1 losses into the connection cryostats. In the quench experiment, BFPP1 losses were deliberately shifted inside a dipole using an orbit bump, and the heat deposition in the magnet was increased in steps by reducing the beam separation. The dipole eventually quenched at a luminosity of 2.3×10^{27} cm^{-2} s^{-1}. Results from particle shower simulations indicate that the peak power density achieved during the test was around 15-20 mW/cm^3. The test is planned to be repeated in another location in Run 3 to further reduce the quench level uncertainty. These results scaled to 7 TeV – taking into account the changes of quench limits from 6.37 TeV to 7 TeV – confirmed that BFPP1 ions would limit the luminosity to less than 2.0×10^{27} cm^{-2} s^{-1}, well below the HL-LHC target of 7×10^{27}cm^{-2} s^{-1} and therefore would limit the full exploitation of the ALICE upgrade.

To eliminate any risk of ion-induced quenches in the DS next to IR2, it is foreseen to install TCLD collimators, as shown schematically in Figure 5-7. One collimator per side of the ALICE experiment is

sufficient to intercept the secondary beams from the most dominant processes (BFPP1 and EMD1) in a location where these ions are well separated from the main beam. The baseline for IR2 is to install the collimator in the connection cryostat in Cell 11 and to implement a closed orbit bump. The bump makes the BFPP1 beam miss the aperture at the first maximum of the locally generated dispersion since IP2 and redirects the beam onto the TCLD jaw. At the same time, the EMD1 beam, which carries ~65 W at a luminosity of $7 \times 10^{27} \mathrm{cm}^{-2}\ \mathrm{s}^{-1}$, could be intercepted with the other jaw. The feasibility of operating with closed orbit bumps of a few mm over more than 100 m has been successfully demonstrated in the 2015 Pb-Pb run [83], as well as in the 2018 Pb-Pb run [84].

The collimator length (60 cm) and material (Inermet 180) are the same as for the TCLDs around IR7 to optimize the TCLD production and spare plans. Particle shower simulations suggest that, with such jaws, the power deposition density in the coils of downstream magnets is expected to remain below 1 $\mathrm{mW/cm}^3$ if the BFPP1 and EMD1 beams impact at least 2 mm from the collimator edges. Hence there is no risk that the showers escaping from the jaws induce a quench of the downstream magnets or of the bus bars [82][85].

5.4.4 Dispersion suppressors around IR1/5

The ATLAS and CMS target luminosity for heavy ion operation in the HL-LHC is the same as for ALICE ($7 \times 10^{27} \mathrm{cm}^{-2}\ \mathrm{s}^{-1}$) [9]. The situation in IR1/5 is, however, different from IR2 since the BFPP1 ions produced in IP1/5 are lost towards the end of the last dipole in Cell 11. As the loss location is close to the connection cryostat, the risk of quenches can be mitigated by redirecting the losses onto the cryostat beam screen using local orbit bumps [57]. Such bumps have been routinely used in the 2015 [83] and 2018 [84] Pb-Pb runs at 6.37 Z TeV, enabling peak luminosities up to $6.2 \times 10^{27}\ \mathrm{cm}^{-2}\ \mathrm{s}^{-1}$. This is a robust solution, providing sufficient margin for the HL-LHC goal [81][82]. Losing the ions in the connection cryostat also reduces the total heat load to be evacuated by the cryogenic system. A significant fraction of the power is expected to be deposited in the Pb shielding of the connection cryostat, which is less critical than the power deposited in the cold mass of magnets as the Pb shielding is mainly thermalized to the thermal screen (~60-65K) [81][82].

Losses in the DS regions also occur during proton operation. Power deposition studies however indicate that there is no risk that these protons quench DS magnets in the HL-LHC operation. At the HL-LHC proton-proton design luminosity of $5 \times 10^{34}\ \mathrm{cm}^{-2}\ \mathrm{s}^{-1}$, the predicted power density in DS magnet coils is 1-2 $\mathrm{mW/cm}^3$, which is safely below the magnet quench level [47]. This remains true for the ultimate luminosity value of $7.5 \times 10^{34}\ \mathrm{cm}^{-2}\ \mathrm{s}^{-1}$ that caused 50% larger peak losses. The long-term dose in the magnet coils reaches about 20 MGy for an integrated luminosity of 3000 fb^{-1} [47]. Also, this is considered acceptable since magnets are expected to sustain a peak dose up to about 30 MGy. The proton simulation studies for the DS are discussed in more detail in Chapter 10. Based on these results, it is concluded that, like for heavy ions, no DS collimators around IR1/5 are needed for proton operation. These collimators are therefore not part of the HL-LHC baseline.

5.4.5 Dispersion suppressor collimator design

The TCLD (see Figure 5-8) consists of two parallel jaws collimating the beam in the horizontal plane. The TCLD design is identical for IR7 and IR2. Some design choices are driven by the more constrained installation between 11T dipoles around IR7. In both cases, the active material of the jaws was chosen to be the heavy tungsten alloy Inermet 180 because the TCLD will rarely be exposed to a large beam load, hence there is no need at this stage to consider advanced materials, while optimising the absorption in the given longitudinal constraints is important. As for all new collimators, the design includes BPMs. The jaws are water cooled, using squared 9 mm pipes. In this compact design, the maximum jaw opening reaches 25 mm from the beam centre, 5 mm less than for standard collimators. The TCLD will be integrated in a specially designed assembly, containing a beam pipe for the other beam, as well as a cryo-bypass (see Refs. [86] [87] and references therein).

Table 5-6: Key parameters of TCLD collimators

Characteristics	Units	Value
Jaw active length	mm	600
Jaw absorbing material	-	Inermet 180
Flange-to-flange distance	mm	1080
Number of jaws	-	Two
Orientation	-	Horizontal
Number of BPMs per jaw	-	Two
RF damping	-	RF fingers
Cooling of the jaw	-	Yes
Cooling of the vacuum tank	-	No
Minimum gap	mm	< 2
Maximum gap	mm	50
Stroke across zero	mm	5
Number of motors per jaw	-	Two
Angular adjustment	-	Yes
Transverse jaw movement (fifth axis)	-	No

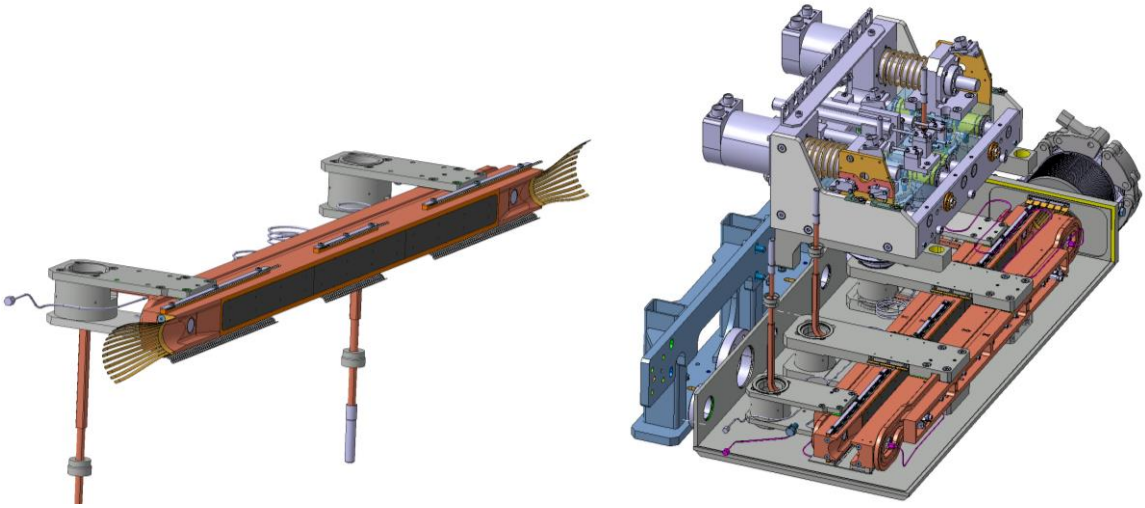

Figure 5-8: TCLD collimator jaw. The present design foresees a 60 cm-long jaw made of tungsten heavy alloy. The figure also shows RF fingers, cooling pipes and BPMs. Courtesy of L. Gentini.

5.5 Upgrades for impedance improvement

5.5.1 Introduction and rationale

The LHC impedance budget is largely dominated by the contribution of the LHC collimators [1] that amounts to more than 90% in the frequency of interest. For this reason, the present collimation system has been conceived in a way that it can be easily upgraded to reduce the impedance, since every secondary collimator slot TCSG in IR3 and IR7 features a companion slot TCSM for the future installation of a low-impedance secondary collimator [1]. A total of 22 slots (IR7) and 8 slots (IR3) are already cabled* for a quick installation

* Present installations include cabling for the collimator controls, but not for the read-out of the in-jaw BPMs, which were not part of the collimator design when these slots for system upgrade were prepared. Also missing are the last meters of radiation-hard cabling from the tunnel cable trails to the collimators.

of new collimators – referred to as TCSPM – that can either replace or supplement the present TCSG collimators. A partial preparation of these slots was done in LS1.

The importance of minimizing the machine impedance for the HL-LHC has been emphasized in Refs. [89] [90] [91], and in the 2013 LHC collimation review [76]. It is also important to stress that each new TCS collimator will also add the BPM functionality for a faster setup, We therefore foresee that, by the time of the full HL-LHC implementation (LS3), some or all of the available TCSM slots will be equipped with advanced collimators using new jaw materials with thin coating layers, to reduce the machine impedance. A staged installation using LS2 and LS3 is the present installation baseline (see Section 5.5.2). Simulations predict that beam stability can be re-established for all the HL-LHC scenarios if the CFC of present secondary collimators is replaced, at least in the betatron cleaning insertion, with a jaw material having an electrical conductivity a factor of 50 to 100 higher than CFC [89][90].

Secondary collimators in IR7 play a crucial role in LHC machine protection and might be exposed to large beam losses. Therefore, collimator materials and designs must also be robust against beam failure (at least those exposed to horizontal losses). The driving requirements for the development of new materials are thus: (i) low resistive-wall impedance to avoid beam instabilities; (ii) high cleaning efficiency; (iii) high geometrical stability to maintain the extreme precision of the collimator jaw during operation despite temperature changes; and (iv) high structural robustness in case of accidental events like single-turn losses. The latter requirement rules out the possibility to deploy high-Z metals because of their relatively low melting point and comparatively large thermal expansion that impairs their resistance to thermal shocks [92]. The present baseline for the upgraded secondary collimators relies on novel carbon-based materials such as molybdenum carbide-graphite (MoGr), a ceramic composite, jointly developed by CERN and Brevetti Bizz (IT), in which the presence of carbides and carbon fibres strongly catalyses the graphitic ordering of carbon during high temperature processing, enhancing its thermal and electrical properties [93][94]. To further improve their surface electrical conductivity, these materials will be coated with pure molybdenum.

In addition to the impedance improvements, the new TCSPM design also features a number of improvements in the mechanical design (see Figure 5-9) [95]. They incorporate the BPM button design. The key hardware parameters are listed in Table 5-7.

Table 5-7: Parameters of TCSPM collimators

Characteristics	**Units**	**Value**
Jaw active length	mm	1000
Jaw material	-	MoGr
Flange-to-flange distance	mm	1480
Number of jaws	-	2
Orientation	-	Horizontal, vertical, skew
Number of motors per jaw	-	Two
Number of BPM buttons per jaw	-	Two
RF damping	-	Fingers
Cooling of the jaw	-	Yes
Cooling of the vacuum tank	-	Yes
Minimum gap	mm	< 1
Maximum gap	mm	60
Stroke across zero	mm	5
Angular adjustment	-	Yes
Jaw coating	-	Yes: Mo
Transverse jaw movement (fifth axis)	mm	± 10

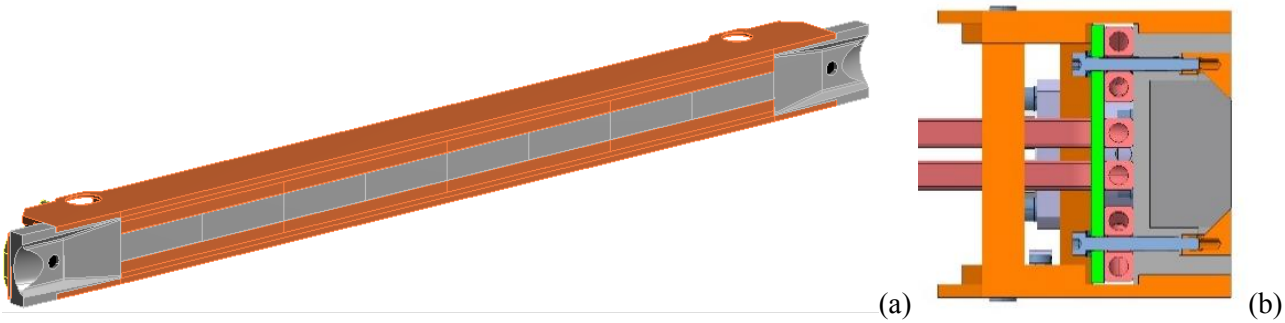

Figure 5-9: The 3D view of the TCSMP jaw (a) and its cross-section (b).

5.5.2 Staged installation

The present low-impedance upgrade baseline foresees the installation of TCSPM collimators in 9 out of 11 TCSM slots per beam. Two slots out of the original upgrade pool have been dropped for cost optimisation, in light of recent estimates that indicate that this revised baseline is compatible with the HL-LHC goals. Each TCSM slot sits immediately downstream of the respective TCSG slot, where regular TCSG collimators are installed. The installation is foreseen in two stages: a first installation in the Long Shutdown 2 (LS2), involving 4 TCSPM collimators per beam, followed by a second installation in LS3, when the remaining 5 collimators per beam will be installed. Assets of this choice are:

- It provides an important reduction of the collimator impedance already for the LHC Run 3, when the upgraded beam parameters from the LHC Injector Upgrade (LIU) program will progressively become available. This allows studying the impedance limitations for the HL-LHC.
- It allows possible further iterations on the new collimator design for LS3.
- It allows distributing resources that would otherwise have to be made available in LS3, when WP5 will be focused on the IR1/5 upgrade.

The choice of the slots for installation during LS2 [96] was mainly driven by maximising the impedance reduction for the first upgrade phase with the limited pool of upgraded collimators; the expected thermo-mechanical loads on the new collimators in case of regular or abnormal losses have also been taken into account. In terms of cleaning inefficiency, numerical simulations have shown that all the considered options are equivalent. The optimisation process highlighted that:

- The first two skew collimators were not selected. They are the most loaded secondary collimators and are exposed to large jaw deformations in the HL-LHC. A new design that mitigates jaw deformation is necessary for these collimators.

The risk of damage for the present slots, in case of injection failures or asynchronous dumps, is considered tolerable [96].Table 5-8 details the installation slots of the TCSPM collimators in LS2. In general, the installation slots are always the TCSM ones and the present TCSGs are kept operational, with the only exceptions being those slots where test hardware is already installed and foreseen for future use (e.g. in D4L7.B1 and D4R7.B2). The choice of the two TCSG that will not be replaced is being studied by exploring various options.

Table 5-8: Installation slots of the TCSPM collimators in LS2, along with the collimation angle [96].

B1 slot	B2 slot	Angle [deg]
TCSG.D4L7.B1	TCSG.D4R7.B2	90.0
TCSM.B4L7.B1	TCSM.B4R7.B2	0.0
TCSM.E5R7.B1	TCSM.E5L7.B2	130.5
TCSM.6R7.B1	TCSM.6L7.B2	0.5

5.5.3 Validation of new design

The new collimator design [95] along with novel materials and coating solutions must be validated for operation in the LHC. For this purpose, a rich program of validation tests has been carried out involving mechanical engineering prototyping, validation of new materials for operation with HUV and at high radiation doses, and tests with high radiation doses (e.g. at BNL and GSI) [101]. HiRadMat tests [99][100] demonstrated among other things that a full-scale MoGr jaw could withstand the most challenging design failure scenario (injection error) without apparent damage and that the Mo-coating layer exhibited only a small, non-catastrophic surface scratch which can be compensated for by exposing an undamaged surface to the beam using the 5th axis functionality[†]. Furthermore, tests with circulating beam in the LHC have been carried out in 2017–2018 with a special prototype built with MoGr bulk and with three stripes with different surface (uncoated MoGr, Mo coating and TiN coating [102][103]. The measured tune shift confirms a significantly lower impedance, although a discrepancy with numerical simulations can be explained by the quality of the microstructure of the coating and of the jaw roughness. This aspect has been improved for the series production. The prototype collimator was successfully used in regular operation throughout 2018 without issues [104][105].

5.5.4 Reduction of impedance of primary collimators

The WP5 impedance upgrade includes a contribution to the procurement of low-impedance material for the primary collimators that are otherwise renewed under the Consolidation project. In LS2, 4 primary collimators of IR7, the horizontal one and the vertical one for both beams, will be replaced with the new design called TCPPM that adds [106]: (1) MoGr absorbing material, without coating; (2) BPM functionality. For the case of primary collimators continuously exposed to primary beam losses, coating the active jaw part is not considered a viable option. The MoGr provides an improvement of about a factor 5 in resistivity compared to CFC, while ensuring a similar robustness against beam failure. Five TCPPM are built in LS2, 4 for the machine and one spare. The HL-LHC-WP5 contributes by procuring material for 3 collimators.

5.6 Advanced concepts for collimation upgrade recently integrated into the baseline

In this Section we discuss two new collimation concepts and designs that were integrated in the WP5 upgrade baseline in Dec. 2019: crystal collimation for heavy-ion beams and hollow electron lenses (HELs). These two items, which are schematically illustrated in Figure 5-10, were part of the approved studies within WP5 and became in 2019 part of the HL-LHC Baseline through in-kind contributions from Russia. Focus was put in recent years to review the needs for these upgrades for the HL-LHC and to demonstrate the required technology in tests without and with beam. Both crystal collimation and HELs address, in different ways, further improvements of the betatron collimation system.

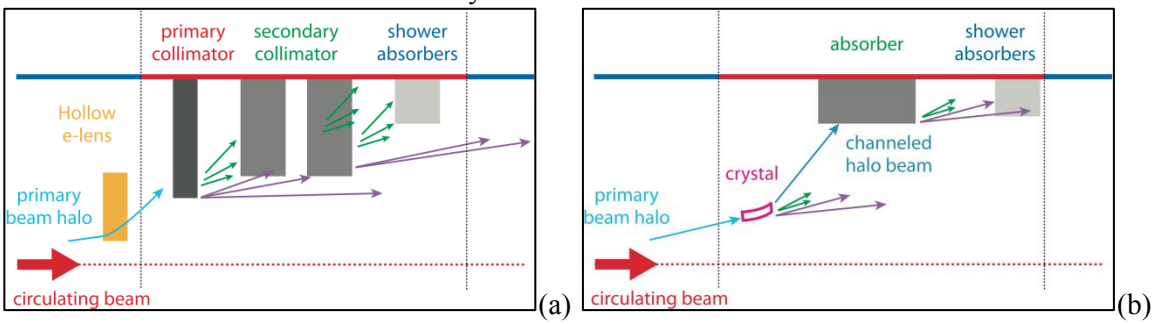

Figure 5-10: Illustrative view (a) of the collimation system with integrated hollow e-lens or equivalent halo diffusion mechanism; (b) an ideal crystal-based collimation.

[†] Observations of jaw surface damage are not straightforward. In case of failure, dedicated beam measurements (e.g., check of alignment positions found with beam-based techniques, impedance measurements) will be setup to see if any detrimental effect is observed compared to the reference system.

5.6.1 Hollow electron lenses for enhanced halo collimation

Operational experience in 2012 indicates that the LHC collimation would profit from halo control mechanisms. The operation of Run 2 at 6.5 TeV showed a less severe impact from halo losses [107]; however, scaling them to HL-LHC beam parameters is still a source of concerns. In particular, the presence of over-populated tails in the LHC beams was consistently observed in dedicated measurements at the LHC [107]. Simple extrapolations to the HL-LHC beam intensities lead to the estimate that more than 30 MJ can be stored at transverse amplitudes between 3.5-4.0 σ and the aperture of primary collimators. This scenario, in particular considering that crab-cavities might produce new fast-loss failures at the HL-LHC, requires the need for an active control of tail population at the HL-LHC. The HEL described in this Section are the most promising solution to achieve this goal. These aspects were reviewed in various international WP5 reviews that recommended the insertion of HEL in the WP5 upgrade baseline [108][109].

In a HEL, a hollow electron beam runs parallel and concentrically to the proton or ion beam. The hollow beam produces an electromagnetic field only affecting halo particles above a given transverse amplitude determined by its inner radius, changing their transverse diffusion speed. The conceptual working principle and its integration into the collimation system are illustrated in Figure 5-10 (a). A solid experimental basis achieved at the Tevatron indicates that this solution is promising for the LHC ([110] and references therein). The potential advantages of the electron lens collimation are several:

- Control of the primary loss rates, with potential mitigation of peak loss rates in the cold magnets, for a given collimation cleaning. Peak power losses on the collimators themselves can be optimized as well.
- Controlled depletion of beam tails (mitigate risk of damage with tens of MJ in the tails).
- Mitigation of loss spikes in the case of orbit drifts.
- Scrape the beam at very low amplitudes (>3 σ) without the risk of damage, as one would have for bulk scrapers.
- Tuning of the impact parameters on the primary collimators with a possible improvement in cleaning efficiency (in particular for ions).
- Possibility to tighten primary collimator settings for a smaller β^* reach, through reduced beam tails.

IR4 is considered to be the best candidate for installing the two HEL devices due to the larger than standard inter-beam distance that eases integration aspects, cryogenics availability, low-radiation environment, and quasi-round beams.

The HEL is targeted at enabling active control of beam tails above 3 to 4 real beam sigmas, with tail depletion efficiencies of the order of 90% over times of tens of seconds. This should be possible, ideally, in all phases of the operational cycle, but specifically at top energy. No specific loss problems are expected at injection energy, but the possibility to use HELs at 450 GeV is considered as a key asset for an efficient commissioning of these complex devices, that is required to be able to perform tail depletion during the beam energy ramp before reaching 7 TeV. The present parameters of the HL-LHC lenses, optimized for 7 TeV, are given in Table 5-9. Note that the HEL design should ensure: (i) the possibility of pulsing the current turn-by-turn (as required to drive linear resonances in the machine before beams are in collision); (ii) a train-by-train selective excitation (leaving 'witness' trains with populated halos for diagnostics and machine protection purposes). The present design of the HL-LHC lenses is shown in Figure 5-11, and a preliminary integration in IR4 is given in Figure 5-12.

Table 5-9: Hollow electron beam equipment parameters

Parameter	Value
Geometry	
Length of the interaction region, L (m)	3
Desidered transverse scraping range (σ, ε= 2.5 μm)	3.5 – 7.1
Inner/outer electron beam radii at 7 TeV (mm)	1,1 – 2.2
Inner/outer cryostat diameter (mm)	132/ ≈ 500
Inner vacuum chamber diameter (mm)	60
Magnetic fields at 7 TeV and magnet parameters	
Main solenoid field, B_m (T)	5
Gun solenoid field, B_g (T)	0.35
Bending Solenoid field (T)	3.5
Compresor factor $\sqrt{B_m/B_g}$	3.8
Maximum current in main solenoid (A)	250 - 300
Electron gun	
Inner/outer cathode diameters (mm)	8.0 – 16.0
Peak yield at 10 kV, I (A)	5
High-voltage modulator	
Cathode-anode voltage (KV)	10
Cathode-ground voltage (KV)	15
Rise time (10% - 90%) (ns)	200
Repetiotion rate (kHz)	35

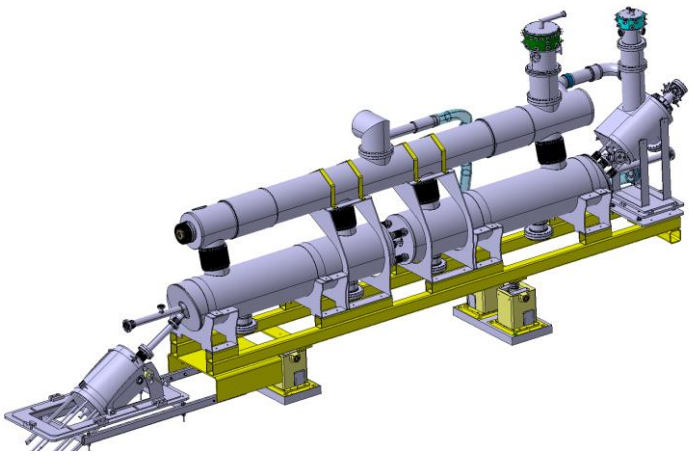

Figure 5-11: 3D design of the HL-LHC hollow e-lens. An ‘S’ shape is proposed. Courtesy of D. Perini.

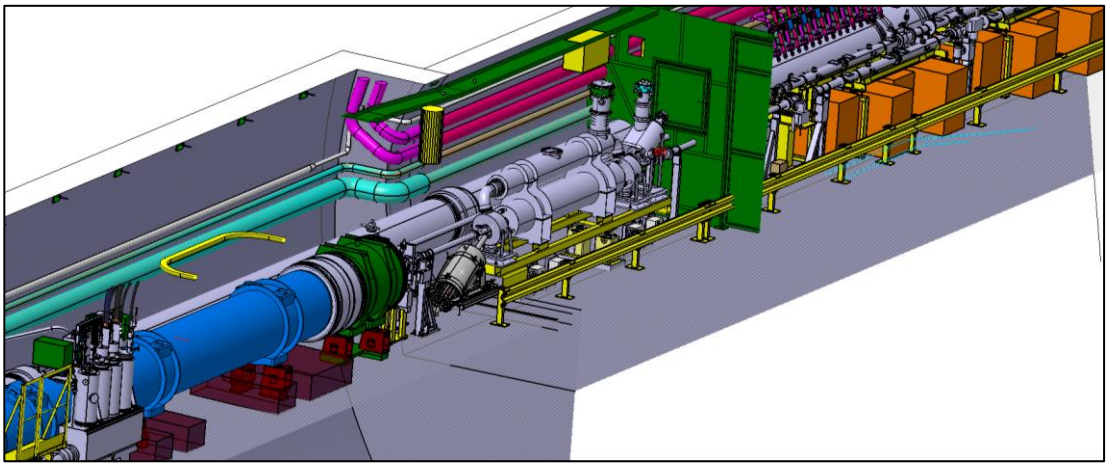

Figure 5-12: 3D integration in P4 for the HEL of beam 1 [109].

5.6.2 Crystal collimation

Highly pure bent crystals can be used to steer high-energy particles that get trapped by the potential of parallel lattice planes. Equivalent bending fields of up to hundreds of Tesla can be achieved in crystals with a length of only a few mm, which allows, in principle, steering halo particles to a well-defined point where dedicated absorbers are located. This scheme is shown schematically in Figure 5-10 (b). As opposed to the standard multi-stage collimation system based on amorphous materials, requiring several secondary collimators and absorbers to catch the products developed through the interaction with matter (see Figure 5-1), one single absorber per collimation plane is in theory sufficient in a crystal-based collimation system.

Simulations indicate a possible gain in cleaning efficiency for proton beams by a factor 5 to 10 [112], even for a layout without an optimized absorber design. In the present layout, this can only be achieved with low beam intensities because deploying crystal collimation for proton beam would require adding in IR7 new – to be designed – absorbers for the ~ 1 MW halo. The crystal collimation option is particularly interesting for collimating heavy-ion beams, where more stringent limitations are expected (see Section 5.4.2) and where the implied losses in IR7 are compatible with the existing hardware and layout in IR7. The recent R&D program on crystal collimation has been focused on ion beam performance, to demonstrate the feasibility of this concept. A unique crystal collimation test stand has been available for beam tests at high energy in the LHC during Run 2 [112]. A summary of the main results can be found in the contributions to the Crystal Collimation Day organized on October 18th, 2018 [114] (see Refs. [115] [116] [117]). Additional important results were achieved during the 2018 heavy ion run, in November 2018, showing an improvement of ion collimation cleaning by up to a factor 7 [118][119]. The LHC beam tests also validated critical hardware components like the high-precision goniometer and its controls that allow maintaining the crystal angular orientation at the optimum value for channelling with sub-μrad resolution. Continuous channelling was achieved during energy ramp and betatron squeeze.

The specifications of the crystal devices are given in Ref. [112] and summarized in Table 5-10. The present IR7 layouts include two different design versions, with the newest design installed in 2016 and 2017 featuring improvements obtained after the first installation in 2015. A newer, final version is now available [121] and it is being prototyped during LS2. For a complete system, it is ideally required to have a total of eight crystals: two per beam and per plane, allowing one to confine possible orbit drifts of both signs while ensuring a good cleaning performance. The test stand in IR7 only has 4, with one crystal only per beam plane.

During LS2, it was decided to integrate crystal collimation in the upgrade baseline in order to cope with potential schedule issues with the production of the new 11 T dipoles for IR7 (see Section 5.4.2). The proposal was approved by the management in Dec. 2019, thanks to the possibility to build the new required hardware through an in-kind contribution by Russia. The detailed scope of this upgrade consists in preparing 4 new

crystal primary collimators (TCPCs) that can replace the existing 4 devices installed in IR7[‡]. The latter were conceived for MD studies and not for regular operations, which calls for an improvement of their design. The controls also need to be upgraded in order to adapt the operational modes to the standards used by the rest of the collimation system for operations with high intensity beams. The WP5 teams are presently working on a schedule for a possible installation of the new devices before the end of LS2, with the fall-back option to install them (or complete the installation, if fewer can be installed in LS2) in a subsequent end-of-year shutdown.

Table 5-10: Crystal equipment parameters.

Parameter	Value
Crystal length along the beam	4 ± 0.1 mm
Total height	< 55 mm
Total weight	< 150 g[§]
Channeling plane	<110>
Channeling axis	<111> or <110>
Miscut for planar channeling	< 40 µrad
Torsion	< 1 µrad/mm
Bending	50.0 ± 2.5 µrad
Miscut for axial channeling	0 ± 18 mrad
Dislocation density	< 1 cm^2

5.7 Other collimators from the present system required in the HL-LHC

It is important to realize that several devices of the present LHC collimators, which are not to be modified or replaced in the collimation upgrade baseline described above, must remain reliably operational for the HL-LHC era. A summary is given in Table 5-11. These items are subject of consolidation of the system that is not discussed as part of this document.

Table 5-11: Collimators of the present system that remains operational in Run 3 and Run 4.

Functional type	Type	Plane	Material	BPM	Run 2	Run 3	Run 4
Primary IR3	TCP	H	CFC	No	2	2	2
Secondary IR3	TCSG	H	CFC	No	8	8	8
Absorber IR3	TCLA	H, V	W alloy	No	8	8	8
Primary IR7	TCP	H, V, S	CFC	No	6	2	2
Secondary IR7	TCSG	H, V, S	CFC	No	22	14	4
Absorber IR7	TCLA	H, V	W alloy	No	10	10	10
Tertiary IR1/2/5/8	TCTP	H, V	W alloy	Yes	16	16	16
Physics debris absorbers IR1/5	TCL	H	Cu, W alloy	No	12	12	0

5.8 Acknowledgements

This Chapter reports on important contributions by several people who, across the years, participated to the collimation upgrade studies. The authors who took the role to summarize all these contributions on behalf of the WP5 teams, would like to kindly acknowledge all the work done by these teams over the year.

5.9 References

[1] O. Brüning (Ed.) *et al.*, LHC Design Report Vol. 1 (2004). DOI: 10.5170/CERN-2004-003-V-1.

[2] R. Assman *et al.*, The final collimation system for the LHC, CERN-LHC-PROJECT-REPORT-919.

[‡] As a part of the in-kind contributions, devices for a 8-TCPC system will be built, but the IR7 upgrade baseline does not include CERN budget for the infrastructure preparation.

[§] 300 g might be accepted following the results on goniometer studies.

[3] R. Bruce *et al.*, LHC Operation Workshop, Evian, 2011. INDICO: 155520.

[4] R. Bruce, et al., Sources of machine-induced background in the ATLAS and CMS detectors at the CERN Large Hadron Collider, Nucl. Instrum. Methods Phys. Res. A729 DOI: 10.1016/j.nima.2013.03.058.

[5] G. Valentino *et al.*, Beam diffusion measurements using collimator scans in the LHC, *Phys. Rev. Spec. Top. Accel. Beams* **16** (2013) 021003. DOI: 10.1103/PhysRevSTAB.16.021003.

[6] K. H. Mess and M. Seidel, Collimators as diagnostic tools in the proton machine of HERA, *Nucl. Instrum. Meth*. A351 (1994) 279–285. DOI: 10.1016/0168-9002(94)91354-4.

[7] H. Burkhardt, *et al.* Collimation System, Conference (2013). DOI: 10.5170/CERN-2015-005.109.

[8] S. Redaelli *et al.*, LHC Collimator Controls for a Safe LHC Operation, wepmu020.

[9] Z. Citron *et al.*, Future physics opportunities for high-density QCD at the LHC with heavy-ion and proton beams, CERN-LPCC-2018-07 (2018).

[10] G. Apollinari, I. Béjar Alonso, O. Brüning, P. Fessia, M. Lamont, L. Rossi, L. Tavian, High-Luminosity Large Hadron Collider (HL-LHC) Technical Design Report V. 0.1 DOI: 10.23731/CYRM-2017-004.

[11] 4th HL-LHC/LIU Cost & Schedule Review 2019 Close-out presentation EDMS: 2271479 (Confidential)

[12] B. Salvachua Ferrando *et al.*, Cleaning performance of the LHC collimation system up to 4 TeV mopwo048.

[13] N. Fuster *et al.*, Collimation, Proc. 9th LHC Operations Evian Workshop, Evian, France (2019).

[14] S. Redaelli *et al.*, Replacement of TCT in IR1, IR2, IR5 and of TCSG Collimators in IR6 with Collimators with Embedded BPM Buttons, EDMS: 1251162, CERN, Geneva, Switzerland (2013).

[15] A. Bertarelli *et al.*, The Mechanical Design for the LHC Collimators, moplt008.

[16] S. Redaelli *et al.*, Final Implementation and Performance of the LHC Collimator Control System, Proc. PAC09, Vancouver (CA). Conference: C09-05-04, FR5REP007.

[17] A. Bertarelli *et al.*, Mechanical design for robustness of the LHC collimators, Proc. PAC2005, Knoxville. TPAP004.

[18] S. Redaelli, Change of number of low-impedance secondary collimators for HL-LHC EDMS: 2165931.

[19] R. Bruce, R.W. Assmann and S.Redaelli, Calculations of safe collimator settings and β* at the Large Hadron Collider, *Phys. Rev. ST Accel. Beams* **18**, (2015). DOI : 10.1103/PhysRevSTAB.18.061001.

[20] R. Bruce *et al.*, Reaching record-low β^* at the CERN Large Hadron Collider using a novel scheme of collimator settings and optics, *Nucl. Instrum. Methods Phys. Res. A* **848** (2017). DOI: 10.1016/j.nima.2016.12.039.

[21] F. Carra *et al.*, LHC collimators with embedded beam position monitors: A new advanced mechanical design, Proc. IPAC2011, San Sebastian, IPAC-2011-TUPS035 (2011).

[22] D. Wollmann *et al.*, Beam feasibility study of a collimator with in-jaw beam position monitors, *Nucl. Instrum. Methods Phys. Res., Sect. A* **768**, 62, (2014). DOI: 10.1016/j.nima.2014.09.024.

[23] G. Valentino *et al.*, Successive approximation algorithm for BPM-based LHC collimator alignment, *Phys. Rev. ST Accel. Beams* **17**, 021005 (2014). DOI: 10.1103/PhysRevSTAB.17.021005.

[24] G. Valentino *et al.*, Final implementation, commissioning, and performance of embedded collimator beam position monitors in the Large Hadron Collider, *Phys. Rev. Accel. Beams* **20**, 081002 (2017) DOI: 10.1103/PhysRevAccelBeams.20.081002.

[25] R. Bruce *et al.*, Installation of a primary collimator with orbit pickups (TCPP) replacing a TCP, LHC-TC-EC-0005, EDMS: 1705737, CERN, Geneva, Switzerland (2016).

[26] R. Bruce and S. Redaelli, Installation of a low-impedance secondary collimator (TCSPM) in IR7, LHC-TC-EC-0006, EDMS: 1705738, CERN, Geneva, Switzerland (2016).

[27] A. Rossi *et al.*, Installation of two wire collimators in IP1 for Long Range Beam-Beam compensation, LHC-TC-EC-0009, EDMS: 1832270, CERN, Geneva, Switzerland (2017).

[28] A. Rossi *et al.*, Installation of two wire collimators in IP5 for Long Range Beam-Beam compensation, LH-TC-EC-0007, EDMS: 1705791, CERN, Geneva, Switzerland (2018).

[29] R. Bruce *et al.*, Machine Configuration, Proc. 9th LHC Operations Evian Workshop, Evian, France (2019), in publication.

[30] D. Wollmann *et al.*, First beam results for a collimator with in-jaw beam position monitors, Proc. IPAC2011. THPZ027.

[31] D. Wollmann *et al.*, Experimental verification for a collimator with in-jaw beam position monitors, Proc. HB2012. mop242.

[32] R. Bruce *et al.*, Sources of machine-induced background in the ATLAS and CMS detectors at the CERN Large Hadron Collider, *Nucl. Instrum. Methods Phys. Res., Sect. A* **729**, 825 (2013). DOI: 10.1016/j.nima.2013.03.058.

[33] ATLAS Collaboration, Characterisation and mitigation of beam-induced backgrounds observed in the ATLAS detector during the 2011 proton-proton run, *J. Instrum.* **8**, P07004 (2013). DOI: 10.1088/1748-0221/8/07/P07004.

[34] ATLAS Collaboration, Comparison of simulated and observed LHC beam backgrounds in the ATLAS experiment at E_{beam} = 4 TeV, *J. Instrum.* **13**, P12006 (2018). DOI: 10.1088/1748-0221/13/12/P12006.

[35] R. Bruce *et al.*, Collimation-induced experimental background studies at the CERN Large Hadron Collider, *Phys. Rev. Accel. Beams* **22**, 021004 (2019). DOI: 10.1103/PhysRevAccelBeams.22.021004.

[36] A. Bertarelli *et al.*, An experiment to test advanced materials impacted by intense proton pulses at CERN HiRadMat facility, *Nucl. Instr. Meth. B* **308** (2013) 88. CERN-ATS-Note-2013-005 TECH.

[37] G. Gobbi *et al.*, Novel LHC collimator materials: High-energy Hadron beam impact tests and nondestructive postirradiation examination, *Mechanics of Advanced Materials and Structures* 1-13, DOI: 10.1080/15376494.2018.1518501.

[38] R. De Maria *et al.*, SixTrack V and Running Environment, *Int. J. Mod. Phys. A*, DOI: 10.1142/S0217751X19420351.

[39] A. Mereghetti *et al.*, SixTrack for cleaning studies: 2017 updates, Proc. 8th Int. Particle Accelerator Conf. (IPAC'17), Copenhagen, Denmark, 2017. DOI: 10.18429/JACoW-IPAC2017-THPAB046.

[40] D. Mirarchi *et al.*, "Cleaning Performance of the Collimation System of the High Luminosity Large Hadron Collider", in Proc. 7th Int. Particle Accelerator Conf. (IPAC'16), Busan, Korea, May 2016, pp. 2494-2497. DOI: 10.18429/JACoW-IPAC2016-WEPMW030.

[41] H. Garcia Morales *et al.*, Beam cleaning of the incoming beam in experimental IRs in HL-LHC, CERN-ACC-NOTE-2017-0023, 2017.

[42] E. Quaranta *et al.*, Modeling of beam-induced damage of the LHC tertiary collimators, *Phys. Rev. Accel. Beams* **20**, 091002 (2017). DOI: 10.1103/PhysRevAccelBeams.20.091002.

[43] R. Bruce *et al.*, Triplet and TCT protection during asynchronous dump in HL-LHC, presentation at the 7th HL-LHC annual meeting 2017, CIEMAT, Madrid, Spain.

[44] A. Tsinganis *et al.*, Impact on the HL-LHC triplet region and experiments from asynchronous beam dumps on tertiary collimators, Proc. 8th Int. Particle Accelerator Conference, Copenhagen, Denmark, (2017). DOI: 10.18429/JACoW-IPAC2017-MOPAB011.

[45] C. Bertella *et al.*, Study of damages induced on ATLAS silicon by fast extracted and intense proton beam irradiation, *Nucl. Instrum. Methods Phys. Res., Sect. A* **924**, pp. 236-240 (2019). DOI: 10.1016/j.nima.2018.06.043.

[46] M. Mentink, Conservative Quench Scenario Considerations in the IT Main Circuit and Impact on Voltages to Ground, presentation at the Magnet circuit forum 20th February 2018, CERN, INDICO: 704894.

[47] F. Cerutti *et al.*, IR collimation upgrades - outgoing beam, presentation at the International Review of the HL-LHC collimation system 2019, INDICO: 780182.

[48] L.S. Esposito and F. Cerutti, "Energy deposition for HL-LHC v1.1: TAN/D2/Q4", Presentation at the 4th Joint HiLumi LHC-LARP Annual Meeting, Tsukuba Japan, 2014.

[49] R. de Maria, Update on tolerance for remote alignment in IR1/5 for HL-LHC, presentation at the Collimation Upgrade Specification Meeting #108, 2018, INDICO: 757667.

[50] P. Fessia, Remote alignment options and solutions, Presentation at the 61st HL-LHC TCC, 15th November 2018, INDICO: 772120.

[51] 67th Collimation Upgrade Specification Meeting (ColUSM), Feb. 6th, 2016. INDICO: 493012.

[52] HiLumi-WP5 deliverable document 5.4. Available on the collimation page web page.

[53] Web site: Review of 11 T dipoles and cold collimation. INDICO: 155408.

[54] R. W. Assmann *et al.*, Collimator losses in the DS of IR7 and quench test at 3.5 TeV, CERN-ATS-Note-2011-042-MD (2011).

[55] R. W. Assmann *et al.*, Pb ions Collimator losses in the DS of IR7 and quench test at 3.5 Z TeV, CERN-ATS-Note-2012-081-MD (2012).

[56] B. Salvachua *et al.*, Collimation quench test with 4 TeV proton beams, CERN-ACC-NOTE-2014-0036.

[57] J.M. Jowett *et al.*, "Bound-free pair production in LHC Pb-Pb operation at 6.37 Z TeV per beam", Proceedings of IPAC2016, Busan, Korea. DOI: 10.18429/JACoW-IPAC2016-TUPMW028.

[58] B. Salvachua *et al.*, Collimation quench test with 6.5 TeV proton beams, CERN-ACC-NOTE-2016-0015 (2016).

[59] P. D. Hermes *et al.*, LHC Heavy-Ion Collimation Quench Test at 6.37Z TeV, CERN-ACC-Note-2016-0031 (2016).

[60] P. D. Hermes, Heavy-ion collimation at the Large Hadron Collider - Simulations and measurements, Ph.D. thesis, University of Munster, DE (2016) CERN-THESIS-2016-230.

[61] A. Ferrari, P.R. Sala, A. Fasso`, and J. Ranft, FLUKA: a multi-particle transport code, (2005), DOI: 10.2172/877507, 10.5170/CERN-2005-010.

[62] G. Battistoni *et al.*, Overview of the FLUKA code, *Annals of Nuclear Energy* **82**, 10-18 (2015) DOI: 10.1016/j.anucene.2014.11.007.

[63] P. D. Hermes, Tracking simulations of heavy ions quench test, presentation at the 201st LHC Collimation Working Group, 7th March 2016, INDICO: 504706.

[64] A. Mereghetti, Tracking simulations of protons quench test, presentation at the 201st LHC Collimation Working Group, 7th March 2016, INDICO: 504706.

[65] E Skordis *et al.*, FLUKA coupling to SixTrack, Proc. ICFA Mini-Workshop on Tracking for Collimation in Particle Accelerators, CERN, Geneva, Switzerland (2015). DOI: 10.23732/CYRCP-2018-002.205

[66] A. Mereghetti, Performance evaluation of the SPS scraping system in view of the High Luminosity LHC, Ph.D. Thesis, University of Manchester, UK (2015). CERN-THESIS-2015-116.

[67] E. Skordis *et al.*, Impact of Beam Losses in the LHC Collimation Regions, Proceedings of IPAC15, Richmond, VA, USA (2015). CERN-ACC-2015-271.

[68] C. Bahamonde Castro *et al.*, Energy deposition from collimation losses in the DS region at P7, Presentation at the 8th HL-LHC Collaboration Meeting, CERN (2018).

[69] C. Bahamonde Castro *et al.*, Update on energy deposition for IR7 for HL-LHC, presentation at the 7th HL-LHC Collaboration Meeting, Madrid, Spain (2017).

[70] G. Steele *et al.*, Heat load scenarios and protection levels for ions, presentation at the 2013 LHC Collimation Project review. INDICO: 251588.

[71] A. Lechner *et al.*, Energy deposition with cryo-collimators in IR2 (ions) and IR7, presentation at the 3rd Joint HiLumi LHC-LARP Annual Meeting, Daresbury (UK), 2013. INDICO: 257368.

[72] E. Skordis, Updated power deposition simulations for DS collimators in IR7 (proton operation), presentation at the 51st Collimation Upgrade Specification Meeting. INDICO: 366694.

[73] P. D. Hermes, Ion simulations for different TCLD layouts, presentation at the 89th ColUSM, June 16th, 2017. INDICO: 646799.

[74] D. Mirarchi, Proton Simulations for different TCLD layouts, presentation at the 94th ColUSM, Sep. 29th, 2017. INDICO: 666560.

[75] LHC Collimation Review 2009. INDICO: 55195.

[76] 2013 Collimation Project Review. INDICO: 251588.

[77] L. Bottura *et al.*, Expected performance of 11 T and MB dipole considering the cooling performance, presentation at the 8th HL-LHC Collaboration Meeting, CERN, 2018.

[78] L. Bottura *et al.*, Quench performance and assumptions: magnets and cryogenics, presentation at the International Review of the HL-LHC Collimation System (2019). INDICO: 780182.

[79] J.M. Jowett *et al.*, Heavy ion beams in the LHC, Proc. PAC 2003, Portland (2003), TPPB029.

[80] R. Bruce *et al.*, Beam losses from ultraperipheral nuclear collisions between $^{208}Pb^{82+}$ ions in the Large Hadron Collider and their alleviation, *Phys. Rev. ST Accel. Beams* **12** (2009) DOI: 10.1103/PhysRevSTAB.12.071002.

[81] A. Lechner *et al.*, "BFPP losses in the connection cryostat: power deposition and dose estimates for Run 2 (and some outlook to HL-LHC)", Presentation at the LMC Meeting, Sept 2015, INDICO: 442208.

[82] C. Bahamonde Castro *et al.*, Power deposition in LHC magnets due to bound-free pair production in the experimental insertions, Proceedings of IPAC2016, Busan, Korea. DOI: 10.18429/JACoW-IPAC2016-TUPMW006.

[83] J.M. Jowett *et al.*, "The 2015 heavy-ion run of the LHC", Proceedings of IPAC16, Busan, Korea, TUPMW027, pp. 1493-1496. DOI: 10.18429/JACoW-IPAC2016-TUPMW027.

[84] J.M. Jowett *et al.*, "Overview of ion runs during run 2", Proc. 9th LHC Operations Evian Workshop, Evian, France (2019).

[85] C. Bahamonde Castro *et al.*, "Needs for shielding in the connection cryostats in IR2 DS", Presentation at the 14th Meeting of the HL-TCC, Sept 2016, INDICO: 559125.

[86] R. Bruce, A. Mereghetti and S. Redaelli, Installation in IR2 of Dispersion Suppressor Collimators (TCLD), LHC-TC-EC-0012, EDMS: 1973010, CERN, Geneva, Switzerland (2018).

[87] R. Bruce, A. Mereghetti and S. Redaelli, Installation in IR7 of Dispersion Suppressor Collimators (TCLD), LHC-TC-EC-0013, EDMS: 1973028, CERN, Geneva, Switzerland (2018).

[88] G. Steele *et al.*, Preliminary results of the FLUKA TCLD study (IR7), presentation at the Collimation Upgrade Specification Meeting , 18th October 2013, INDICO: 278104.

[89] N. Mounet, Transverse impedance in the HL-LHC era, presentation at the 3rd HiLumi Annual meeting, Daresbury, (2013). INDICO: 257368.

[90] N. Biancacci, presentation at the 55th meeting of the Collimation Upgrade Specification working group INDICO: 390114.

[91] HiLumi WP2 milestone document M29, Initial estimate of machine impedance. CERN-ACC-2014-0005.

[92] A. Bertarelli, Beam Induced Damage Mechanisms and Their Calculation, proceedings of the Joint International Accelerator School on Beam Loss and Accelerator Protection, Newport Beach, DOI: 10.5170/CERN-2016-002.

[93] A. Bertarelli *et al.*, Novel Materials for Collimators at LHC and its Upgrades, HB2014, East Lansing, 2014. CERN-ACC-2015-0173.

[94] A. Bertarelli *et al.*, Development and testing of novel advanced materials with very high thermal shock resistance, Tungsten, Refractory and Hard metals Conference, Orlando, 2014.

[95] F. Carra *et al.*, Mechanical engineering and design of novel collimators for HL-LHC, IPAC2014, Dresden, (2014). DOI: 10.18429/JACoW-IPAC2014-MOPRO116.

[96] S. Antipov *et al.*, Staged implementation of low-impedance collimation in IR7: plans for LS2, CERN-ACC-2019-0001, CERN, Geneva, Switzerland (2019). CERN-ACC-NOTE-2019-0001.

[97] E. Metral, *et al.*, Impedance models, operational experience and expected limitations, presentation at the International Review of the HL-LHC Collimation System (2019). INDICO: 780182.

[98] X. Buffat *et al.*, MD3288 – Instability latency with controlled noise, presentation at the LSWG meeting, 3rd July 2018, CERN, Geneva, Switzerland.

[99] E. Quaranta *et al.*, Towards optimum material choices for HL-LHC collimation upgrade, IPAC2016, wepmw031.

[100] 96th Collimator Upgrade Specification Meeting, 8th November 2017, CERN, Geneva, Switzerland. INDICO: 676105.

[101] E. Quaranta *et al.*, Radiation-induced effects on LHC collimator materials under extreme beam conditions, IPAC2016, wepmw032.

[102] R. Bruce and S. Redaelli, Installation of a low-impedance secondary collimator (TCSPM), LHC-TC-EC-0006, EDMS: 1705738.

[103] S. Antipov *et al.*, Single-collimator tune shift measurement of the three-stripe collimator at LHC, Proceedings of IPAC2018, Vancouver, BC, Canada. DOI: 10.18429/JACoW-IPAC2018-THPAF035.

[104] M. Patecki and A. Mereghetti, Operational experience with the TCSPM prototype, presentation at the 239th LHC Collimation Working Group Meeting, 4th February 2019, INDICO: 792567.

[105] A. Mereghetti *et al.*, Performance of new designs deployed in Run II and plans for Run III, Presentation at the International Review of the HL-LHC Collimation System, INDICO: 780182.

[106] R. Bruce, A. Mereghetti and S. Redaelli, LHC-TC-EC-0016, EDMS: 1973590 (2018).

[107] B. Salvachua Ferrando *et al.*, Beam losses, lifetime and operational experience at 6.5 TeV, Presentation at the International Review of the HL-LHC Collimation System, INDICO: 780182.

[108] Review of the needs for a hollow e-lens for the HL-LHC, 6th – 7th October 2016, CERN, Geneva, Switzerland. INDICO: 567839.

[109] International review on the e-lens concept readiness for integration into the HL-LHC baseline, 19th – 20th October 2017, CERN, Geneva, Switzerland. INDICO: 648237.

[110] G. Stancari, Electron-lens experience at Tevatron and RHIC, International review on the e-lens concept readiness for integration into the HL-LHC baseline, 19th – 20th October 2017, CERN, Geneva, Switzerland.

[111] M. Fitterer, *et al.*, Resonant and random excitations on the proton beam in the Large Hadron Collider for active halo control with pulsed hollow electron lenses arXiv:1804.07418.

[112] D. Mirarchi *et al.*, Design and implementation of a crystal collimation test stand at the Large Hadron Collider, *The European Physical Journal C* **77:424** (2017). DOI: 10.1140/epjc/s10052-017-4985-4.

[113] C. Bahamonde Castro *et al.*, Simulations of energy deposition for crystal collimation, Presentation at the 106th ColUSM Meeting, INDICO: 740297.

[114] HL-LHC Crystal Collimation Day, INDICO: 752062.

[115] D. Mirarchi *et al.*, Recent results on crystal collimation for a low-background physics run at the LHC, Presentation at the HL-LHC Crystal Collimation Day, INDICO: 752062.

[116] M. D'Andrea *et al.*, LHC operational experience with proton beams, Presentation at the HL-LHC Crystal Collimation Day, INDICO: 752062.

[117] R. Rossi *et al.*, LHC operational experience with heavy ion beams, Presentation at the HL-LHC Crystal Collimation Day, INDICO: 752062.

[118] D. Mirarchi *et al.*, Crystal collimation for lead ion beams, Presentation at the International Review of the HL-LHC Collimation System, INDICO: 780182.

[119] M. D'Andrea *et al.*, Preliminary results from crystal collimation studies in 2018, Presentation at the 70th HL-LHC TCC, INDICO: 804616.

[120] W. Scandale et al., Observation of channeling for 6500 GeV/ c protons in the crystal assisted collimation setup for LHC, *Phys. Lett. B* **758** (2016) 129-133.DOI: 10.1016/j.physletb.2016.05.004.

[121] I. Lamas Garcia *et al.*, "Update on mechanical design for crystal collimators", Presentation at the 111th ColUSM Meeting, INDICO: 788971.

[122] R. Bruce, A. Mereghetti and S. Redaelli, LHC-TCAP-EC-0001, EDMS: 1973905 (2018).

[123] P. Fessia *et al.*, LHC-MW-EC-0002, EDMS : 1321045.